



Published in final edited form as:

ACS Nano. 2010 January 26; 4(1): 267–278. doi:10.1021/nn901393v.

## Combining Chemoselective Ligation with Polyhistidine-Driven Self-Assembly for the Modular Display of Biomolecules on Quantum Dots

Duane E. Prasuhn<sup>1</sup>, Juan B. Blanco-Canosa<sup>3</sup>, Gary J. Vora<sup>1</sup>, James B. Delehanty<sup>1</sup>, Kimihiro Susumu<sup>2</sup>, Bing C. Mei<sup>2</sup>, Philip E. Dawson<sup>3</sup>, and Igor L. Medintz<sup>1,\*</sup>

<sup>1</sup>Center for Bio/Molecular Science and Engineering, Code 6900

<sup>2</sup>Division of Optical Sciences, Code 5611, U.S. Naval Research Laboratory, Washington, DC 20375

<sup>3</sup>Departments of Cell Biology & Chemistry and the Skaggs Institute for Chemical Biology, The Scripps Research Institute, La Jolla, CA 92037

### Abstract

One of the principle hurdles to wider incorporation of semiconductor quantum dots (QDs) in biology is the lack of facile linkage chemistries to create different types of functional QD-bioconjugates. A two-step modular strategy for the presentation of biomolecules on CdSe/ZnS core/shell QDs is described here which utilizes a chemoselective, aniline-catalyzed hydrazone coupling chemistry to append hexahistidine sequences onto peptides and DNA. This specifically provides them the ability to ratiometrically self-assemble to hydrophilic QDs. The versatility of this labeling approach was highlighted by ligating proteolytic substrate peptides, an oligoarginine cell-penetrating peptide, or a DNA-probe to cognate hexahistidine peptidyl sequences. The modularity allowed subsequently self-assembled QD constructs to engage in different types of targeted bioassays. The self-assembly and photophysical properties of individual QD conjugates were first confirmed by gel electrophoresis and Förster resonance energy transfer analysis. QD-dye-labeled peptide conjugates were then used as biosensors to quantitatively monitor the proteolytic activity of caspase-3 or elastase enzymes from different species. These sensors allowed the determination of the corresponding kinetic parameters, including the Michaelis constant ( $K_M$ ) and the maximum proteolytic activity ( $V_{max}$ ). QDs decorated with cell-penetrating peptides were shown to be successfully internalized by HEK 293T/17 cells, while nanocrystals displaying peptide-DNA conjugates were utilized as fluorescent probes in hybridization microarray assays. This modular approach for displaying peptides or DNA on QDs may be extended to other more complex biomolecules such as proteins or utilized with different types of nanoparticle materials.

### Keywords

quantum dot; nanocrystal; peptide; DNA; chemoselective ligation; bioconjugation; hybridization; cellular delivery; polyhistidine; self-assembly

---

\*igor.medintz@nrl.navy.mil, Phone: 202-404-6046, Fax: 202-767-9594.

## Introduction

Due to their unique photophysical properties, luminescent semiconductor nanocrystals or quantum dots (QDs) have become well-established fluorophores for many *in vitro* and *in vivo* bioapplications.<sup>1-3</sup> QDs have also enabled the monitoring of multiple, specific biological molecules simultaneously (i.e., multiplexing),<sup>4-6</sup> something that has not been easily achievable to date. Although investigations utilizing QD fluorophores have already provided valuable research insight into fundamental cellular processes such as endocytosis and vesicle fusion,<sup>7,8</sup> the major obstacle to their further utility continues to be the limited set of modification chemistries available for creating disparate QD-bioconjugates in a controlled manner. Most approaches target a limited set of functionalities for QD biomodification and result in little control over the loading number and/or spatial orientation of the attached biomolecules. For example, carboxylated QDs are often coupled to the ubiquitous amines available in protein sequences using carbodiimide (EDC) chemistry,<sup>9</sup> however, this requires a vast excess of reactants, commonly results in heterogeneous attachment with concomitant mixed avidity, and/or is prone to cross-linking and aggregation due to insoluble intermediates.<sup>10</sup> Biotin-Avidin chemistry is constrained by the need to label both participants appropriately, equal susceptibility to cross-linking, and the presence of the large multivalent Avidin protein (64 kDa) intermediaries in the conjugate.<sup>9</sup> With some exceptions,<sup>11</sup> adsorption or non-covalent association (through electrostatic or hydrophobic interactions) of natural/engineered proteins or nucleic acids generally yields poor control over substrate loadings and heterogeneity in spatial orientation and avidity.<sup>1,2,12</sup> Clearly, QD conjugation chemistries are needed that are efficient and targeted, utilize functionalities orthogonal to common biological moieties (i.e., do not cross-react), minimize heterogeneity in attachment, and allow for control over conjugate loadings.

In the past few years, we have developed an alternative method for QD biofunctionalization driven by the metal-affinity interactions between the Zn-rich surface of CdSe/ZnS core/shell QDs and the imidazole groups of polyhistidine-appended biomolecules.<sup>13</sup> The interaction occurs rapidly, is equally efficient using QDs capped with either negatively charged or neutral ligands, has high affinity equilibrium binding constants for solution self-assembly ( $K_d^{-1} \sim 10^9 \text{ M}^{-1}$ ),<sup>13</sup> and allows control over the number of substrate molecules arrayed on a single QD through modulation of the molar ratios used.<sup>14,15</sup> In some cases, this self-assembly approach can even provide control over the spatial orientation of the biomolecule on the QD surface.<sup>16</sup> Polyhistidine driven self-assembly has already been used to construct complex QD-biomolecular sensing systems by facilitating the display of recombinant proteins/peptides, chemically modified nucleic acids, and synthetic peptides onto QD surfaces<sup>13,17,18</sup> and has also been successfully implemented by several other research groups.<sup>19-21</sup>

The ability to append polyhistidine sequences to a variety of different target peptides or nucleic acids in a flexible, efficient manner without altering their native sequence or subsequent function could greatly enhance QD bioconjugation. The Dawson lab has recently reported an aniline-catalyzed hydrazone coupling for peptide and protein modification (see Figure 1A).<sup>22-24</sup> In this approach, aniline reacts with the aldehyde to form a highly reactive iminium intermediate that subsequently reacts with the hydrazine moiety to yield the desired

hydrazone product. Significantly, the hydrazine, aldehyde and aniline reactive groups in this chemistry are orthogonal to most common biological functionalities. Although amines react with aldehydes to form imines, these species rapidly hydrolyze in water leaving the amine unmodified. It has been shown that under aniline catalysis, bisaromatic hydrazones have bioconjugation rates of  $10^1 - 10^3 \text{ M}^{-1} \text{ s}^{-1}$  in mild, aqueous buffers (slightly acidic to neutral pH) and proceed to completion within 30 min using 100 mM aniline with 10  $\mu\text{M}$  of reactants.<sup>22-24</sup> The relatively high  $K_{\text{eq}}$  ( $2.3 \times 10^6 \text{ M}^{-1}$ ) together with the slow hydrolysis kinetics ( $k_{-1} = 0.03 \times 10^{-3} \text{ s}^{-1}$ ) in the absence of aniline has made this chemistry of significant utility in bioconjugation. Hydrazone ligation has been applied to the ligation of unprotected peptides and for fluorescent labeling of peptides and proteins.<sup>22-24</sup> Cumulatively, these properties suggest that aniline-catalyzed hydrazone ligation could be useful for the selective biofunctionalization of QDs.

Here we present a two-step, modular approach for the general attachment of peptides and nucleic acid oligomers onto QD surfaces (Figure 1B). First, a hexahistidine ( $\text{His}_6$ )-appended, 'starter' peptide derivatized with either a hydrazine or aldehyde moiety is reacted with the biomolecule of interest displaying the complementary functionality under chemoselective ligation conditions. Both the  $\text{His}_6$ - 'starter' peptide and its ligation target are site-specifically functionalized with the appropriate complementary reactive groups (hydrazine or aldehyde) at their termini to ensure the covalent chemistry has minimal impact on the ultimate function. Purified conjugates were then self-assembled to QD particles at the desired equivalents to yield the final QD-biomolecular conjugates. Gel electrophoresis and analysis of Förster resonance energy transfer (FRET) interactions between the central QD and proximal dye-labeled ligands verified successful self-assembly. The utility of these QD-biomolecular conjugates were demonstrated in a variety of targeted biosensing, hybridization and cellular uptake assays.

## Results and Discussion

### Chemoselective Ligation and Self-assembly to QDs

A detailed description of the reactants and synthetic conditions can be found in the Materials and Methods section. As shown in Figure 2, four ligation substrates of interest were synthesized: two peptides containing proteolytic cleavage sites recognized by elastase (**1a**) or caspase-3 (**1b**); a DNA oligomer probe complementary to the cholera *ctxA* gene (**1c**);<sup>25</sup> and a synthetic cell-penetrating peptide (CPP) expressing the canonical TAT-based polyarginine motif (**1d**). Substrates **1a-c** were pre-labeled with fluorescent dyes (Texas Red, AlexaFluor555, and tetramethylrhodamine A (TAMRA), respectively) to facilitate subsequent FRET-based interactions. Peptides **1a**, **1b**, and **1d** each displayed a terminal 2-hydrazinonicotinoyl group (HYNIC), while DNA oligomer **1c** ended in a 4-formylbenzoyl group (4FB, prepared from 5'-aminoylated-DNA using *N*-hydroxysuccinimide ester chemistry) for use in the chemoselective ligation.

Conjugate **3** (composed of the  $\text{His}_6$ -appended, linker peptide **2a** and the elastase proteolytic substrate **1a**) was prepared using standard conditions developed for aniline-catalyzed hydrazone coupling.<sup>22-24</sup> **1a** and **2a** were reacted at equimolar concentrations (1 mM) with 100 mM aniline under slightly acidic conditions (0.1 M  $\text{NH}_4\text{OAc}$ , pH 5.5) at room

temperature overnight. Purification on Ni-NTA agarose resin and desalting on an oligonucleotide purification cartridge (OPC) yielded **3**, the elastase substrate flanked by the Texas Red dye and the His<sub>6</sub> sequence. Using similar conditions, conjugate **4**, an AlexaFluor555/His<sub>6</sub>-labeled caspase-3 substrate, was obtained from the reaction of **1b** with **2a**. To emphasize the modularity of the methodology, two additional starter peptides were utilized, **2b** which has a highly homologous sequence to **2a** (single additional alanine difference) but displays a terminal HYNIC group, and **2c** which combines a polyproline spacer between the His<sub>6</sub> and the 4FB group. Starter peptide **2b** was ligated to modified-DNA strand **1c** yielding conjugate **5**, the His<sub>6</sub>-appended DNA probe. Both TAMRA labeled and unlabeled versions of the DNA were used equally effectively in this reaction. Starter peptide **2c** was ligated to the HYNIC-modified CPP **1d** to yield conjugate **6**, the His<sub>6</sub>-appended CPP.

Several benefits are inherent to the ligation and purification strategy described here for joining peptides or DNA to other peptides. Reactions are typically carried out in small volumes ranging from 20 to 100  $\mu$ Ls thus minimizing reagent consumption. Allowing the ligations to proceed overnight can provide access to almost complete conjugation efficiency (>95%).<sup>22–24</sup> We noted that adding an excess of either reactant did not appear to improve the overall yield. These efficiencies are important, as in many cases, the biological molecule being utilized (peptides, proteins, DNA) and QDs are costly and only available in small volumes of sub mM concentrations. Thus, the labeling reactions must of necessity be highly chemoselective, rapid and efficient in terms of yield. Reactions worked equally efficient regardless of whether the biomolecule of interest was labeled with the 4FB or HYNIC group. This interchangeability may be important for reactions targeting multiple peptides or DNA in the same reaction mixture and for similar modification of other more diverse and/or 'reactive' biomolecules which may not tolerate the proximity of such groups for long periods of time. Purification over Ni-NTA agarose resin allowed the capture of only the His<sub>6</sub>-peptide labeled products while removing all other reactants. The subsequent desalting step allowed long-term storage of the lyophilized conjugates aliquots which could be reconstituted in any buffer system as needed. We found that QD-conjugates could be stably self-assembled following months of both reactant and ligate storage (10–50 nanomole aliquots) or even shipping across the continental United States. Thus materials can be synthesized, ligated, and stored for use on an 'as needed' basis.

To further accentuate the modularity of the design, the ligated conjugates were self-assembled to QDs of different sizes/emissions capped with both negatively-charged DHLA or neutral DHLA-PEG<sub>600</sub> ligands (Figure 1C).<sup>11,26</sup> Self-assembly of all peptide- and DNA-QD conjugates was verified by performing agarose gel electrophoresis and subsequent FRET characterization (*vide infra*). Electropherograms of DHLA-QDs incubated with peptide- and DNA-ligates confirmed self-assembly and control over the molar ratio of ligate attached to the QDs by the changes in relative migration rates (data not shown). These results are similar to those observed and reported for gel separations of other self-assembled QD–DNA/protein conjugates.<sup>27,28</sup> We also note that despite DNA conjugate **5** and DHLA-functionalized QD surfaces both being strongly negatively charged, the appended His<sub>6</sub>-sequence can still facilitate efficient self-assembly analogous to previous findings.<sup>17</sup>

## FRET Analysis of QD-Dye Conjugates

FRET interactions between the central QD donors and self-assembled dye-labeled versions of the peptide/DNA ligates were also examined. This served to confirm self-assembly, help characterize the QD-conjugate structures, and provided a basis for subsequent FRET-based proteolytic monitoring. Acceptor dyes were chosen to provide substantial spectral overlap with particular QD donors. Conjugate **3** (labeled with Texas Red) was self-assembled to 550 nm emitting QDs, **4** (labeled with AlexaFluor555) to 520 nm QDs, and DNA conjugate **5** (labeled with TAMRA) was coordinated to 550 nm QDs, all of which were capped with DHLA. The absorption and emission spectra for each QD-donor dye-acceptor pair are shown in Figures 3A–C. Table 1 lists the photophysical properties for the QD-conjugates including the calculated Förster radii ( $R_0$ ) for each system, which are centered around 50 Å. FRET interactions were monitored while discretely increasing the ratio of dye-labeled ligate self-assembled per QD donor in the ensemble. Figures 3D–F show the QD photoluminescence (PL) and background/direct-acceptor excitation corrected emission spectra collected for each system as acceptor valence increases. Figures 3G–I present the corresponding normalized plots of the loss in QD donor PL vs. acceptor ratio, corresponding FRET efficiency  $E$  along with a Poisson correction to account for heterogeneity during self-assembly (see Materials and Methods), and the sensitized acceptor reemission for each system. QD donor-dye acceptor center-to-center separation distances ( $r$ ) as determined from analysis of the QD donor data are presented in Table 1. Within each conjugate a significant decrease in QD donor PL is noted as acceptor valence increases and all are >50% quenched at ratios of <5 acceptors per donor confirming efficient FRET in each system. The highest quenching is noted in the 520 nm QD-AlexaFluor555 pair where the QD donor is ~90% quenched at a nominal valence of ~2 acceptors/QD although this system has the least favorable  $R_0$  value. This may reflect a combination of the acceptors high absorptivity along with a particular conformation assumed by peptide **4** placing the acceptor closer to the QD. Similarly, the 550 nm QD-Texas Red conjugate **3** system also derives an  $r$  value suggesting that the peptide conformation places the acceptor dye quite close to the QD surface.

The corresponding sensitized acceptor-emission observed for each system was rather modest with the highest sensitization of ~0.4 achieved in the 550 nm QD-TAMRA system. This most likely reflects the fact that, although each acceptor dye is capable of efficiently quenching its particular QD donor, the energy transferred is dissipated by a number of decay channels, most of which are non-radiative. Only a portion of the transferred energy is radiatively emitted and this is well below unity. This result is not uncommon and has been noted in a number of other QD donor-dye acceptor systems.<sup>17, 29</sup> The rate of sensitized emission for each acceptor can also be expected to fluctuate and will be influenced by a combination of its photophysical properties, its environment, and the method of attachment. This variability means that the best estimation of FRET efficiency is consistently derived from the analysis of changes in the QD donor as utilized here.<sup>30</sup> As the FRET systems described above utilized DHLA-QDs, for comparative purposes, we also self-assembled Texas Red-conjugate **3** to 580 nm emitting QDs functionalized with DHLA-PEG<sub>600</sub> in a similar manner (data not shown). In comparison to the  $r$  value of 30 Å estimated for this peptide with 550 nm DHLA QDs, the redder emitting PEGylated QDs yielded an  $r$  value of 66 Å, more than double. A small portion of this difference, ~4 Å, results from the larger

diameter of the 580 nm QDs. We ascribe the remaining difference to the peptides physical interaction with the far longer DHLA-PEG<sub>600</sub> ligands. Energy-minimization of the ligand structure using modeling software suggests that the PEG structure may extend 25–30 Å away from the QD surface (data not shown) and it is not unexpected that this ligand can interact with and influence the structure of peptides which must penetrate the ligand shell to self-assemble on the QD surface. This also suggests that utilizing such QD-peptide structures may require pretesting with different capping ligands for optimal activity in a targeted biological assay. Verifying dye-acceptor proximity to the QD within each system served to confirm; 1-self-assembly, 2-that we were able to predictably control the loading numbers of ligate self-assembled per QD, and 3-allowed direct tracking of the corresponding intra-assembly FRET efficiency. Overall, the FRET results are quite similar to what we have shown for other self-assembled QD – protein/peptide/DNA systems<sup>14, 17, 31</sup> and are also important for deriving quantitative data in the subsequent proteolytic assays.

### Sensing of Caspase-3 and Elastase Proteolytic Activity

With an understanding of the individual FRET-based quenching properties within the different QD-conjugate systems, we investigated the utility of this conjugation strategy for assembling biosensors capable of monitoring enzymatic proteolysis. Three enzymes were targeted, caspase-3 and two elastase enzymes of either human or porcine origin. Caspase-3 or apopain is a cysteine-aspartic acid protease that functions downstream during the execution-phase of cellular apoptosis by specifically cleaving targeted substrate proteins. Its activity is also down-regulated in different types of tumors and this decreased activity is used as a prognostic indicator of chemosensitivity in breast and ovarian tumors.<sup>32–34</sup> Caspase-3 is also involved in the cleavage of the amyloid-beta 4A pre-protein whose activity is related to neuronal death in Alzheimer's disease. Elastases are serine proteases similar in activity to trypsin and chymotrypsin but are distinguished by their ability to hydrolyze elastin, the major protein in connective tissue whose plasticity allows many tissues to resume their shape after stretching or contracting<sup>35,36</sup>. Aberrant elastase function is associated with several diseases including emphysema and neutropenia. Both caspase-3 and elastases are important pharmaceutical targets; thus, necessitating the ability to monitor their activity in different assay formats.

Prior to performing the proteolytic assays, we utilized the data gathered in Figure 3 panels G,H and in similar experiments as calibration curves. This allowed us to select appropriate ratios of dye-labeled peptide to assemble onto the QD such that a large change in FRET efficiency following cleavage could be measured for each system. Comparing the changes in sensor FRET efficiency following proteolysis to these curves allowed us to transform the FRET recovery data into quantitative velocity values, as demonstrated for similar QD-peptide and protein conjugates<sup>14,37–39</sup>. As the recombinant caspase-3 utilized for testing with the QD-sensors manifests a very high specific activity ( 2,500 U/μg), this assay required utilizing very small amounts of enzyme. Thus, caspase-3 concentration was maintained at 65 U total while 520 nm emitting QDs assembled with an average of 7 AlexaFluor555-labeled conjugate **4** per QD were added to each reaction in increasing concentrations as described in the Materials and Methods section. DHLA-QDs were utilized for this assay as attempts at using QDs functionalized with PEGylated ligands appeared to

hinder enzyme access to the peptides cleavage site (data not shown). The enzymatic curve (Figure 4A) yielded a  $K_M = 8.6 \mu\text{M}$ ,  $V_{\text{max}} = 186 \text{ nM peptide cleaved min}^{-1}$ ,  $k_{\text{cat}} = 22.9 \text{ min}^{-1}$ , and  $k_{\text{cat}}/K_M = 2.7 \times 10^6 \text{ M}^{-1} \text{ min}^{-1}$ . These are quite similar in magnitude to previously reported values of  $K_M = 9.7 - 13.8 \mu\text{M}$ ,  $k_{\text{cat}} = 6.0 - 7.1 \text{ sec}^{-1}$ , and a  $k_{\text{cat}}/K_M = 0.44 - 0.72 \times 10^6 \text{ M}^{-1} \text{ sec}^{-1}$  for the same enzyme determined through a fluorometric assay.<sup>40</sup> They are also close to values collected using 2 similar self-assembled FRET-based QD fluorescent protein sensors ( $K_M = 1.8 - 3.0 \mu\text{M}$ ,  $V_{\text{max}} = 30 - 47 \text{ nM peptide cleaved min}^{-1}$ ,  $k_{\text{cat}}$  of  $1.3 - 2 \text{ sec}^{-1}$ , and  $k_{\text{cat}}/K_M$  of  $7.2 \times 10^7$  and  $6.7 \times 10^7 \text{ M}^{-1} \text{ sec}^{-1}$ ).<sup>37</sup> These consisted of mCherry fluorescent protein-acceptors expressing two different versions of a caspase-3 cleavage site on an extended linker located between the His<sub>6</sub>-QD attachment site and the main protein structure. Interestingly, similar to the current sensor, that QD-fluorescent protein conjugate also required the use of DHLA ligands to allow the enzyme access to the substrate site.

The activity of human neutrophil elastase and porcine pancreatic elastase were assayed using an excess enzyme format as described in the Materials and Methods section. 580 nm DHLA-PEG<sub>600</sub> QDs were self-assembled with an average Texas Red-labeled conjugate **3**:QD ratio of 10. A constant QD concentration of  $0.21 \mu\text{M}$  was maintained while adding increasing concentrations of the enzyme to the reaction mixtures. Analysis of the changes in QD donor emission after the reaction allowed the data to be transformed into the enzymatic activity curves depicted in Figure 4B, C and allowed us to estimate the apparent maximal velocity  $V_{\text{max, app}}$  for each enzyme. Values of  $0.5 \mu\text{M}$  and  $93.6 \text{ nM peptide cleaved min}^{-1}$  were estimated for the porcine pancreatic and human neutrophil elastases, respectively. In this assay, both elastase enzymes were not affected or hindered from recognizing the QD-attached peptide by the presence of PEG solubilizing ligands. Given the nM to  $\mu\text{M}$  differences in the values, it is evident that these types of QD sensing configurations are versatile enough to allow the monitoring of enzymatic activities that differ by orders of magnitude.

### Cellular Uptake of Peptide-Functionalized QDs

With their unique, robust photophysical properties, QDs are particularly appealing fluorophores for the targeted labeling of cells and monitoring of intracellular processes. We thus evaluated this same conjugation method for decorating QDs with polyarginine cell-penetrating peptides (CPP) to facilitate their specific uptake into targeted cells. This approach builds upon our previous work demonstrating that QDs displaying such peptides could be selectively taken up by cells even in media containing other unfunctionalized QDs while manifesting almost no concomitant toxicity.<sup>41</sup> 550 nm emitting QDs surface functionalized with DHLA-PEG<sub>600</sub> were self-assembled with 25 equivalents of conjugate **6** (CPP) or 25 equivalents of **2c** (starter peptide) as a negative control and then exposed to human embryonic kidney (HEK 293T/17) cells for 1 hr incubations. The same cells were concurrently exposed to AlexaFluor647-labeled transferrin (AF647-Tfn) to counter-label the endosomes. The use of PEGylated QDs for cellular uptake is particularly important as charged DHLA QDs can precipitate in the slightly acidic endosomal and cytosolic environments. After washing/fixing the cells and staining the nuclei, the samples were imaged by bright field and epifluorescence microscopy and representative images are shown in Figure 5. In panel A, QD uptake is readily visualized by the strong green fluorescent

emission which co-localizes with the AF647-Tfn in the endosomes. This result was expected as almost all CPP-facilitated delivery of QDs to eukaryotic cells appears to be mediated by the endocytic system.<sup>42</sup> In contrast, cells incubated with QDs displaying self-assembled unligated-starter peptide (**2c**) did not demonstrate any uptake at all (Figure 5B). Clearly, delivery of the peptide conjugate is dependent upon the QDs displaying an accessible polyarginine motif for initial interactions with the cellular membrane. Again, no significant cellular toxicity was noted in cells that underwent QD delivery using such short incubation times and conjugate concentrations (data not shown); similar to what we reported previously.<sup>41</sup>

### Hybridization Microarray Assays

As all the QD-conjugates described to this point utilized only peptide-to-peptide ligation we wished to test the applicability of this chemistry to other non-peptidyl biomolecules. A DNA oligomer with sequence complementarity, to a portion of the *ctxA* toxin gene from the *Vibrionaceae* family<sup>25</sup> was obtained with a 5'-amino modification. This was derivatized to display an aldehyde (**1c**) as described and then chemoselectively ligated to starter peptide **2b** to yield peptido-DNA conjugate **5**. Peptide-DNA hybrids are not uncommon in biochemistry, for example CPP's have been quite frequently conjugated to DNA to facilitate their intracellular delivery.<sup>43</sup> Gel electrophoresis and FRET analysis of TAMRA-acceptor dye labeled versions of **5** (described above) verified that the ligated His<sub>6</sub>-starter peptide portion of the ligate did indeed facilitate efficient assembly of the DNA to QDs. We next applied 0.5 μM solutions of 550 nm QDs self-assembled with 20 equivalents of conjugate **5** (no TAMRA label) as probes for arrays spotted with decreasing concentrations of the *ctxA* gene sequence. Figure 6A depicts representative results obtained using DHLA-PEG<sub>600</sub> QDs, while Figure 6B shows results using DHLA-functionalized QDs. For the DHLA-PEG<sub>600</sub> QD-probes, a limit of detection (LOD) of 10 pmol/μL spotted DNA is obtained while QD-PL intensity appears to increase concomitant to spot concentration. No non-specific hybridization was detected against the non-complementary *ctxB* gene sequence. We also evaluated using DHLA-capped QD probes on an identically prepared slide. In this case, a LOD of 0.4 pmol/μL of spotted DNA is obtained and QD-PL intensity increases with spot concentration to the maximum spotted amount. Again, no non-specific interactions are noted and controls utilizing the same concentration of QDs alone (no assembled peptides) did not result in any significantly observed fluorescence. We ascribe the differences in LOD to the physical presence of the DHLA-PEG<sub>600</sub> molecule on the QD surface which is probably sterically hindering constructive hybridization interactions by blocking some portion of the DNA sequence(s). This, however, may be easily remedied by increasing the length of the DNA sequence such that it expresses a long, non-specific spacer between the QD surface and the region of complementarity, thus allowing the DNA to extend out significantly beyond the PEG-shell surrounding the QD. Additionally, the sensitivity may also be substantially enhanced by exciting the QDs at a significantly bluer wavelength where their absorptivity is considerably higher, rather than at the 543 nm used for the prototype experiments here; this excitation line is close to the QD's absorption minimum.

## Conclusions

We demonstrate here a two-step modular linkage for the multivalent display of peptides and DNA on QD surfaces. Taking advantage of polyhistidine-driven metal-affinity for the Zn-rich surface of QDs, we chemoselectively ligate various functional peptides or DNA to a His<sub>6</sub>-peptidic sequence for subsequent self-assembly to QDs. We have previously experimented with similar types of conjugation, however, those depended primarily on thiol chemistry and we found them to be somewhat limited. The issue arose from the inclusion and targeting of an added cysteine residue adjacent to the His<sub>6</sub>-sequence, thus precluding the presence of other cysteine(s) in the sequence and the added reliance on dithiol reduction and several purification steps along with susceptibility to oxidation.<sup>17,44</sup> The current strategy overcomes this by exploiting the chemoselectivity of aniline-catalyzed hydrazone bond formation between 4FB and HYNIC groups to create the final His<sub>6</sub>-appended bioconjugate. These groups are orthogonal to almost all naturally occurring amino acid functional groups and DNA, are easily appended onto both, and ligate equally well regardless of placement. Furthermore, using the self-assembly of a His<sub>6</sub>-appended bioconjugate can potentially allow a maximum of 50–60 peptides or modified DNA's to be attached to the QD surface with concomitant improvements to avidity.<sup>45</sup>

The modularity and wide applicability of QDs modified with such peptide/DNA-peptide constructs was highlighted by utilizing the QD constructs as proteolytic sensors, as targeted cellular labels, and as hybridization probes. Three different QD emissions were utilized to optimize spectral overlap with given dye-acceptors for FRET analysis and subsequent assays. Conjugates self-assembled equally well with QDs made hydrophilic with either the small charged DHLA or neutral DHLA-PEG<sub>600</sub> surface ligands. The ability to switch between these different ligands and the resulting character of the QDs proved exceedingly important for optimal QD-bioconjugate function. Switching from PEG to the smaller DHLA ligands allowed the caspase-3 enzyme to gain access to the peptides binding site when assembled on the QD and also helped dramatically lower the LOD obtained in the DNA hybridization assay. Although not examined directly here, it is important to note that this approach also provides for some relative control over the spacial orientation of the QD-assembled peptides and DNA. By site-specifically attaching the His<sub>6</sub>-peptide to the terminus of a targeted peptide or DNA, the QD-attachment point is controlled while leaving the remaining active ligate portion available to extend away from the QD surface. This has important implications as in many cases the tertiary structure of ligate is important to overall function. For example, aptamers and similarly functional peptides require folding into a specific structure for recognizing a target and may also necessitate close proximity to the QD for FRET sensing. By specifically ligating to the termini of these molecules and controlling their lateral extension via linker/spacer length, this chemistry can allow for optimal function of such materials when assembled to the QD.

The orthogonality and chemoselectivity of this chemistry offers the possibility for expansion to other nanoparticle systems beyond QDs and can be easily extended to a variety of biomolecules for conjugation. It is not hard to envision gold, iron oxide, or other metallic nanoparticles decorated with surface-functionalizing ligands that terminate in either a hydrazine or aldehyde moiety. Beyond the DNA and peptides examples presented here,

proteins may also be ligated to QDs or other nanoparticles. For this, the proteins can be attached either heterogeneously by targeting their ubiquitous amines, or site-specifically through the incorporation of unnatural amino acids displaying the appropriate functionality.<sup>46,47</sup> In conclusion, as nanoparticle synthesis and the resulting nanomaterials become ever more refined, improved conjugation chemistries will be needed that can deliver 'designer' bioconjugates as desired. Chemoselective ligation methodologies may represent a powerful approach towards this goal.

## Materials and Methods

### Peptides and DNA

Peptide sequences **1a–c**, **2a–c** were prepared using *in situ* neutralization cycles for Boc-solid-phase-peptide synthesis (Boc-SPPS) and modified to express terminal 4-formylbenzoyl (4FB) or 2-hydrazinonictinoyl (HYNIC) functionalities as described.<sup>22,48</sup> Briefly, the peptides were synthesized on 0.1 mmol MBHA resin (4-Methylbenzhydramine, Peptides International, 0.65 mmol/g) using 1.0 mmol of amino acid, 1.0 mmol of HCTU/HOBt, (2-(6-Chloro-1H-benzotriazole-1-yl)-1,1,3,3-tetramethylammonium hexafluorophosphate)/N-hydroxy-benzotriazole (0.4 M solution in dimethylformamide 1:1) and 2 mmol of DIEA (N,N-diisopropylethylamine). Coupling times were typically 1h. Following chain assembly, peptides were cleaved from the resin with HF and 10% of anisole for 1h at 0°C. 4FB was coupled to the N-terminus of the desired peptide in a H<sub>2</sub>O/CH<sub>3</sub>CN solution (1:1) using succinimidyl 4-formylbenzoate (1.5 equiv) and DIEA (7 equiv). All peptides were purified by HPLC and characterized by electrospray ionization mass spectrometry. Prior to any bioconjugation reaction, all peptides were desalted on oligonucleotide purification cartridges (OPC, Applied Biosystems), dried in a DNA120 speed-vacuum (ThermoSavant), and stored as a pellet at –20°C desiccated as described in ref<sup>39</sup>. The 5' amino-modified DNA sequence 5'-cctgccaatccataaccatc-3' **1d** was utilized both with and without tetramethylrhodamine A (TAMRA) labels and was obtained from Operon Biotechnologies, Inc. C<sub>2</sub>-maleimide Texas Red and C<sub>2</sub>-maleimide AlexaFluor555 were obtained from Invitrogen, while *p*-formylbenzoic acid-*N*-hydroxysuccinimide ester was purchased from Research Organics. PD-10 gel permeation columns were obtained from GE Healthcare and Ni-NTA agarose resin from Qiagen. All other reagents were purchased from Acros Organics or Sigma-Aldrich and used as received.

### Quantum Dot Synthesis

CdSe/ZnS core/shell QDs capped with hydrophobic, organic ligands (generally a mixture of trioctylphosphine/trioctylphosphine oxide, TOP/TOPO and hexadecylamine) and having emission maxima centered at ~520, 550, and 580 nm were synthesized using organometallic procedures as previously reported.<sup>11,49,50</sup> The nanocrystals were made water-soluble by exchanging the TOP/TOPO ligands with dihydrolipoic acid (DHLLA) or polyethylene glycol(PEG)-appended DHLLA (PEG with M<sub>W</sub> ~600, DHLLA-PEG<sub>600</sub>) through standard methods, see Figure 1C for structures.<sup>11,26,51,52</sup>

## Bioconjugation and Self-assembly to QD Surface

Peptides containing an elastase proteolytic cleavage site or caspase-3 proteolytic cleavage site were labeled with fluorescent dyes (Texas Red and AlexaFluoro555, respectively) using standard maleimide-cysteine bioconjugation methodology<sup>9</sup> yielding peptides **1a** and **1b**. Aldehyde modified-DNA sequences (**1d**) were obtained by first reacting 0.45 mM DNA (using a 1mM stock solution dissolved in 1x phosphate buffered saline pH 7.4 (PBS, 137 mM NaCl, 10 mM phosphate, 2.7 mM KCl) and 9.09 mM *p*-formylbenzoic acid-*N*-hydroxysuccinimide ester (using a 100 mM stock solution dissolved in DMSO) at room temperature overnight (16–18 hrs). Reactions were then purified on PD-10 gel permeation columns and concentrated in a speed-vac. Concentrations were determined using the dyes molar absorptions (Table 1) and the DNA absorbance  $\epsilon_{260\text{nm}}$  of  $183,430 \text{ M}^{-1} \text{ cm}^{-1}$ . For non dye-labeled peptides, absorption of the conjugated hydrazone bond was utilized ( $\epsilon_{354}=29,000 \text{ M}^{-1} \text{ cm}^{-1}$ ) All absorption spectra were taken on an Agilent Technologies 8453 UV-visible spectrophotometer.

**Chemoselective ligation**—Conjugate **3** was produced through chemoselective ligation using the following procedure. Stocks of peptides **1a** and **2a** (2 mM each) were prepared in 10% DMSO/0.1 M ammonium acetate ( $\text{NH}_4\text{OAc}$ ), pH 5.5. **1a** and **2a** (each at a final concentration 1 mM) were reacted with 100 mM aniline at room temperature overnight in the dark. Resulting conjugate **3** was purified using mini Ni-NTA resin columns, desalted on OPC, quantitated using the Texas Red absorption, dried in a speed-vacuum, and stored as a pellet as described in detail.<sup>39</sup> This generalized procedure was also used to construct conjugates **4**, **5**, and **6**.

**Self-assembly to QDs**—For QD-conjugate self-assembly, His<sub>6</sub>-peptide or DNA-ligates were initially resuspended in 10% DMSO/1x PBS. Each QD-DHLA or QD-DHLA-PEG<sub>600</sub> conjugate was self-assembled by adding the indicated molar ratios of ligate to the QDs in PBS buffer and let incubate for 15 mins to 1 hour prior to use in an assay. QD concentrations were typically 0.2  $\mu\text{M}$  per reaction while varying the ratio of added peptide:QD.

## Fluorescence and FRET Analysis

100  $\mu\text{L}$  aliquots of individual reactions were transferred to 96-well microtiter plates (polystyrene with non-binding surface, Corning). Samples were excited at 300 nm and fluorescence spectra were collected on a Tecan Safire Dual Monochromator Multifunction Microtiter Plate Reader (Tecan, US). Individual spectra were deconvoluted using OriginLab to yield separate background and direct-acceptor excitation corrected QD-donor and dye-acceptor emission profiles for each corresponding peptide:QD ratio. FRET efficiency  $E_n$  ( $n$  = number of dye-acceptors per QD) was determined using:

$$E_n = \frac{(F_D - F_{DA})}{F_D} \quad (1)$$

where  $F_D$  and  $F_{DA}$  are the fluorescence intensities of the donor in the absence and presence of acceptor(s), respectively.<sup>30</sup> Data from FRET efficiency were analyzed using Förster theory to determine values for center-to-center (QD-to-dye) separation distance  $r$  using:

$$r=R_0(n(1-E)/E)^{1/6} \quad (2)$$

$R_0$  designates the Förster distance corresponding to 50% energy transfer for a single donor-acceptor configuration.<sup>30</sup> Expression (2) is applicable to and specifically accounts for the inherent characteristics of a centro-symmetric QD-peptide/DNA-dye conjugate displaying multiple acceptors.<sup>31</sup> To account for the effects of heterogeneity in conjugate valence resulting during self-assembly, in particular at low ratios with high FRET efficiencies, a Poisson distribution function  $p(k,n)$  was used.<sup>15</sup> The FRET efficiency  $E$  in Equation (2) was rewritten as:

$$E(n)=\sum_{k=1}^{\infty}p(k,n)E(k) \text{ with } p(k,n)=\frac{e^{-n}n^k}{k!} \quad (3)$$

where  $n$  is the average acceptor-to-QD ratio used during reagent mixing and  $k$  the exact number of dye-labels conjugated to the QDs.

### Proteolytic Assays

Porcine pancreatic elastase ( $M_W \sim 21.5$  kD, specific activity of 6.6 Units - U/mg, 1 U will hydrolyze 1.0  $\mu\text{mol}$  of N-succinyl-L-Ala-Ala-Ala-*p*-nitroanilide per min at 25 °C, pH 8.0) was obtained from Sigma-Aldrich, while human neutrophil elastase ( $M_W \sim 28.5$  kD, specific activity of 21 U/mg, 1 U will hydrolyze 1.0  $\mu\text{mol}$  of MeO-Suc-Ala-Ala-Pro-Val-*p*-nitroanilide per min at 25°C, pH 8.0) and recombinant human caspase-3 ( $M_W \sim 32$  kD, specific activity of 2,500 U/ $\mu\text{g}$ , 1 unit will cleave 1.0 pmol of the substrate Ac-Asp-Glu-Val-Asp-*p*-nitroanilide per min at 30°C, pH 7.4) were purchased from Calbiochem. For the porcine pancreatic elastase assay, 580 nm QD-DHLA-PEG<sub>600</sub> particles were self-assembled with 10 equivalents of conjugate **3** and aliquoted into a microtiter well plate, diluted (0.5x PBS, pH 7.2), and enzyme was added. The assay was run for 8.5 minutes at 30°C with a constant concentration of 0.21  $\mu\text{M}$  QD substrate per point while enzyme concentration was varied (0.02–2.5  $\mu\text{g}/\mu\text{L}$ ). Samples were run in duplicate or triplicate. Upon completion, the changes in 580 nm QD donor emission were recorded. The human neutrophil elastase sensing assay used similar conditions, but with a reaction time of 20 minutes and an enzyme concentration range of 0.46–475 ng/ $\mu\text{L}$ . For caspase-3 activity assays, 520 nm QD-DHLA was incubated with 7 equivalents of conjugate **4**. A QD stock solution was aliquoted into a microtiter well plate, diluted (0.4x PBS, pH 8.0), and enzyme was added. The assay was run at 30°C for 30 min with a constant enzyme concentration (0.65 U/ $\mu\text{L}$  in 100  $\mu\text{L}$  reactions) while QD substrate concentration was varied (0.01–0.5  $\mu\text{M}$ ). The reactions were quenched with the addition of the alkylating agent  $\alpha$ -iodoacetamide (final concentration of 0.36 mg/mL). The QD donor emission at 520 nm and AlexaFlour 555 emission at 573 nm were then recorded for each point.

Proteolytic cleavage activity or initial rates of enzymatic velocity were determined from changes in QD donor signal or acceptor/QD donor ratios (A/D) as appropriate and compared to a pre-constructed calibration curve for each system where increasing amounts of dye-labeled peptide were self-assembled to QDs under the same condition. A detailed discussion can be found in reference.<sup>14</sup> For assays using an excess substrate format, the maximum reaction rate  $V_{\max}$  and the Michaelis constant  $K_M$  (substrate concentration  $[S]$  at which the reaction proceeds at half the maximum rate) were determined using:<sup>14,37–39</sup>

$$V = \frac{d[P]}{dt} = \frac{V_{\max}[S]}{K_M + [S]} \quad (4)$$

Corresponding turnover number  $k_{\text{cat}} = V_{\max}/[E_{\text{tot}}]$  and molar turnover  $k_{\text{cat}}/K_M$  value were also determined. For assays performed in an excess substrate format, only the apparent maximal velocity  $V_{\max, \text{app}}$  for the concentration of substrate used is reported.

### Cellular Delivery Assays

Cell internalization studies were performed in LabTek™ chambered borosilicate coverglass (Nunc) coated with fibronectin. 550 nm DHLA-PEG<sub>600</sub> QDs pre-incubated with 25 equivalents of conjugate **6** or linker **2c** (negative control) were diluted to 50 nM in complete growth media (Dulbecco's Modified Eagle's medium supplemented with 10% fetal bovine serum) and added to adherent HEK 293T/17 cells (American Type Culture Collection) grown in the chambers. 30 µg/mL AlexaFluoro647-transferrin (AF647-Tfn) was also added to the cells for endosomal labeling (Invitrogen). Cells were incubated with both QD assemblies and Transferrin at 37°C for 1 hr, and then washed once with 1x PBS before fixing with 3% *p*-formaldehyde for 10 minutes at room temperature. The cell nuclei were then stained with DAPI (4',6-diamidino-2-phenylindole, Invitrogen) and washed twice more with PBS. Fixed cells were stored in PBS containing 0.01% sodium azide until imaging. Samples were analyzed by bright field and epifluorescence microscopy using an Olympus IX-71 inverted microscope (60x magnification). Images were collected using a DAPI cube (D350/50× for excitation, dichroic 400DCLP, D460/50m for detection) for nuclear staining, a Cy5 cube (excitation HQ620/60×, dichroic Q660LP, emission HQ700/75m) for the AlexaFluor647-transferrin, and a FITC cube (D470/20× for excitation, 500DCLP) for the 550 nm QDs. Merged images were generated using Adobe Photoshop.

### Microarray Hybridization Assays

Oligonucleotides coding for portions of the cholera toxin  $\alpha$  subunit (*ctxA*) and  $\beta$  subunit (*ctxB*) genes were synthesized with a 5'-amino modifier separated from the oligo by a 12-carbon alkane spacer (Qiagen) and spotted onto aminosilane SuperChip glass slides (Nunc) in 100 mM sodium carbonate/bicarbonate buffer (pH 9.0) at concentrations of 0.08–50 µM using an OmniGrid Accent Contact Printer (Genomic Solutions).<sup>25</sup> Prior to hybridization, spotted microarrays were blocked with a 3% bovine serum albumin-casein solution for 15 min at room temperature and the slides outfitted with MAUI® M4 hybridization chambers (BioMicro® Systems). QD-DNA samples were prepared by incubating 550 nm QD-DHLA or QD-DHLA-PEG<sub>600</sub> particles with 20 equivalents of peptide-DNA conjugates (**5** without

TAMRA modification) as described above. A stock solution of 500 nM DNA-loaded QDs in 1x PBS was applied in 11  $\mu$ L aliquots to the microarrays and allowed to incubate for 3 hours at room temperature on a MAUL Hybridization System (BioMicro<sup>®</sup> Systems). The slides were washed twice post-hybridization with the same buffer for 2 min, rinsed with distilled water, and dried with compressed air. Fluorescent microarray images were captured with a ScanArray Lite confocal laser scanning system (PerkinElmer) using a 543 nm excitation laser. Quantitative comparisons based on emission intensities were made using the ScanArray Express analysis software package (v. 3.0). The emission signal from each microarray element was considered positive only when its quantified intensity was >2x that of the internal negative control elements and >3x the surrounding background.

## Acknowledgments

The authors acknowledge the CB Directorate/Physical S&T Division DTRA/ARO, ONR, NRL, and the NRL-NSI for financial support. D. Prasuhn is supported by an American Society for Engineering Education Fellowship through the Naval Research Laboratory. J.B. Blanco-Canosa gratefully acknowledges the Marie Curie Foundation for a postdoctoral fellowship. P. Dawson is a consultant for Solulink Inc, San Diego, CA.

## References

1. Michalet X, Pinaud FF, Bentolila LA, Tsay JM, Doose S, Li JJ, Sundaresan G, Wu AM, Gambhir SS, Weiss S. Quantum Dots for Live Cells, In Vivo Imaging, and Diagnostics. *Science*. 2005; 307:538–544. [PubMed: 15681376]
2. Klostranec JM, Chan WCW. Quantum Dots in Biological and Biomedical Research: Recent Progress and Present Challenges. *Advanced Materials*. 2006; 18:1953–1964.
3. Algar WR, Massey M, Krull UJ. The Application of Quantum Dots, Gold Nanoparticles and Molecular Switches to Optical Nucleic-Acid Diagnostics. *Trac-Trends in Analytical Chemistry*. 2009; 28:292–306.
4. Goldman ER, Clapp AR, Anderson GP, Uyeda HT, Mauro JM, Medintz IL, Mattoussi H. Multiplexed Toxin Analysis Using Four Colors of Quantum Dot Fluororeagents. *Analytical Chemistry*. 2004; 76:684–688.
5. Medintz IL, Farrell D, Susumu K, Trammell SA, Deschamps JR, Brunel FM, Dawson PE, Mattoussi HM. Multiplex Charge Transfer Interactions Between Quantum Dots and Peptide-Bridged Ruthenium Complexes. *Analytical Chemistry*. 2009; 81:4831–4839.
6. Algar WR, Krull UJ. Towards Multi-Colour Strategies for the Detection of Oligonucleotide Hybridization Using Quantum Dots as Energy Donors in Fluorescence Resonance Energy Transfer (FRET). *Analytica Chimica Acta*. 2007; 581:193–201. [PubMed: 17386444]
7. Zhang Q, Li YL, Tsien RW. The Dynamic Control of Kiss-And-Run and Vesicular Reuse Probed with Single Nanoparticles. *Science*. 2009; 323:1448–1453. [PubMed: 19213879]
8. Lidke DS, Nagy P, Heintzmann R, Arndt-Jovin DJ, Post JN, Grecco HE, Jares-Erijman EA, Jovin TM. Quantum Dot Ligands Provide New Insights Into erbB/HER Receptor-Mediated Signal Transduction. *Nature Biotech*. 2004; 22:198–203.
9. Hermanson, GT. *Bioconjugate Techniques*. 2. Academic Press; San Diego: 2008.
10. Shen H, Jawaid AM, Snee PT. Poly(ethylene glycol) Carbodiimide Coupling Reagents for the Biological and Chemical Functionalization of Water-Soluble Nanoparticles. *ACS Nano*. 2009; 3:915–923. [PubMed: 19275175]
11. Mattoussi H, Mauro JM, Goldman ER, Anderson GP, Sundar VC, Mikulec FV, Bawendi MG. Self-Assembly of CdSe-ZnS Quantum Dot Bioconjugates Using an Engineered Recombinant Protein. *J Am Chem Soc*. 2000; 122:12142–12150.
12. Medintz I, Uyeda H, Goldman E, Mattoussi H. Quantum Dot Bioconjugates for Imaging, Labeling and Sensing. *Nature Materials*. 2005; 4:435–446. [PubMed: 15928695]

13. Sapsford KE, Pons T, Medintz IL, Higashiya S, Brunel FM, Dawson PE, Mattoussi H. Kinetics of Metal-Affinity Driven Self-Assembly Between Proteins or Peptides and CdSe-ZnS Quantum Dots. *J Phys Chem C*. 2007; 111:11528–11538.
14. Medintz IL, Clapp AR, Brunel FM, Tiefenbrunn T, Uyeda HT, Chang EL, Deschamps JR, Dawson PE, Mattoussi H. Proteolytic Activity Monitored by Fluorescence Resonance Energy Transfer Through Quantum-Dot-Peptide Conjugates. *Nature Materials*. 2006; 5:581–589. [PubMed: 16799548]
15. Pons T, Medintz IL, Wang X, English DS, Mattoussi H. Solution-Phase Single Quantum Dot Fluorescence Resonant Energy Transfer Sensing. *J Am Chem Soc*. 2006; 128:15324–15331. [PubMed: 17117885]
16. Medintz IL, Konnert JH, Clapp AR, Stanish I, Twigg ME, Mattoussi H, Mauro JM, Deschamps JR. A Fluorescence Resonance Energy Transfer Derived Structure of a Quantum Dot-Protein Bioconjugate Nanoassembly. *Proc Natl Acad Sci USA*. 2004; 101(26):9612–9617. [PubMed: 15210939]
17. Medintz IL, Berti L, Pons T, Grimes AF, English DS, Alessandrini A, Facci P, Mattoussi H. A Reactive Peptidic Linker for Self-Assembling Hybrid Quantum Dot-DNA Bioconjugates. *Nano Letters*. 2007; 7:1741–1748. [PubMed: 17530814]
18. Pons T, Medintz IL, Sapsford KE, Higashiya S, Grimes AF, English DS, Mattoussi H. On the Quenching of Semiconductor Quantum Dot Photoluminescence by Proximal Gold Nanoparticles. *Nano Letters*. 2007; 7:3157–3164. [PubMed: 17845066]
19. Dennis AM, Bao G. Quantum Dot-Fluorescent Protein Pairs as Novel Fluorescence Resonance Energy Transfer Probes. *Nano Letters*. 2008; 8(5):1439–1445. [PubMed: 18412403]
20. Dif A, Henry E, Artzner F, Baudy-Floc'h M, Schmutz M, Dahan M, Marchi-Artzner V. Interaction between Water-soluble Peptidic CdSe/ZnS Nanocrystals and Membranes: Formation of Hybrid Vesicles and Condensed Lamellar Phases. *J Am Chem Soc*. 2008; 130:8289–8296. [PubMed: 18529051]
21. Liu W, Howarth M, Greytak AB, Zheng Y, Nocera DG, Ting AY, Bawendi MG. Compact Biocompatible Quantum Dots Functionalized for Cellular Imaging. *J Am Chem Soc*. 2008; 130:1274–84. [PubMed: 18177042]
22. Dirksen A, Dawson PE. Rapid Oxime and Hydrazone Ligations with Aromatic Aldehydes for Biomolecular Labeling. *Bioconjugate Chemistry*. 2008; 19:2543–2548. [PubMed: 19053314]
23. Dirksen A, Dirksen S, Hackeng TM, Dawson PE. Nucleophilic Catalysis of Hydrazone Formation and Transamination: Implications for Dynamic Covalent Chemistry. *J Am Chem Soc*. 2006; 128:15602–15603. [PubMed: 17147365]
24. Dirksen A, Hackeng TM, Dawson PE. Nucleophilic Catalysis of Oxime Ligation. *Angew Chem Int Ed Eng*. 2006; 118:7743–7746.
25. Vora GJ, Meador CE, Bird MM, Bopp BC, Andreadis JD, Stenger DA. Microarray-Based Detection of Genetic Heterogeneity, Antimicrobial Resistance and the Viable but Nonculturable State in Human Pathogenic *Vibrio spp*. *Proc Natl Acad Sci USA*. 2005; 102:19109–19114. [PubMed: 16354840]
26. Susumu K, Uyeda HT, Medintz IL, Pons T, Delehanty JB, Mattoussi H. Enhancing the Stability and Biological Functionalities of Quantum Dots via Compact Multifunctional Ligands. *J Am Chem Soc*. 2007; 129:13987–96. [PubMed: 17956097]
27. Medintz IL, Pons T, Delehanty JB, Susumu K, Brunel FM, Dawson PE, Mattoussi H. Intracellular Delivery of Quantum Dot-Protein Cargos Mediated by Cell Penetrating Peptides. *Bioconjugate Chemistry*. 2008; 19:1785–1795. [PubMed: 18681468]
28. Pons T, Uyeda HT, Medintz IL, Mattoussi H. Hydrodynamic Dimensions, Electrophoretic Mobility and Stability of Hydrophilic Quantum Dots. *J Phys Chem B*. 2006; 110:20308–20316. [PubMed: 17034212]
29. Zhang CY, Johnson LW. Quantum-Dot-Based Nanosensor for RRE IIB RNA-Rev Peptide Interaction Assay. *J Am Chem Soc*. 2006; 128:5324–5325. [PubMed: 16620087]
30. Lakowicz, JR. *Principles of Fluorescence Spectroscopy*. 3. Springer; New York: 2006.

31. Clapp AR, Medintz IL, Mauro JM, Fisher BR, Bawendi MG, Mattoussi H. Fluorescence Resonance Energy Transfer Between Quantum Dot Donors and Dye-Labeled Protein Acceptors. *J Am Chem Soc.* 2004; 126:301–310. [PubMed: 14709096]
32. Cohen GM. Caspases: The Executioners of Apoptosis. *Biochem J.* 1997; 326:1–16. [PubMed: 9337844]
33. Louneva N, Cohen JW, Han LY, Talbot K, Wilson RS, Bennett DA, Trojanowski JQ, Arnold SE. Caspase-3 Is Enriched in Postsynaptic Densities and Increased in Alzheimer's Disease. *Am J Pathology.* 2008; 173:1488–1495.
34. Fischer U, Schulze-Osthoff K. New Approaches and Therapeutics Targeting Apoptosis in Disease. *Pharmacological Reviews.* 2005; 57:187–215. [PubMed: 15914467]
35. Paczek L, Michalska W, Bartlomiejczyk I. Trypsin, Elastase, Plasmin and MMP-9 Activity in the Serum During the Human Ageing Process. *Age and Ageing.* 2008; 37:318–323. [PubMed: 18332058]
36. Cantor, JO.; Turino, GM. Elastin and Elastases. Vol. II. CRC; Boca Raton: 1989. p. 159-168.
37. Boeneman K, Mei B, Dennis A, Bao G, Deschamps JR, Mattoussi H, Medintz IL. Sensing Caspase 3 Activity with Quantum Dot-Fluorescent Protein Assemblies. *J Am Chem Soc.* 2009; 131:3828–3829. [PubMed: 19243181]
38. Clapp AR, Goldman ER, Uyeda HT, Chang EL, Whitley JL, Medintz IL. Monitoring of Enzymatic Proteolysis Using Self-Assembled Quantum-Dot Protein Substrate Sensors. *Journal of Sensors.* 2008; 2008:Article # 797436.
39. Sapsford KE, Farrell D, Sun S, Rasooly A, Mattoussi H, Medintz IL. Monitoring of Enzymatic Proteolysis on a Electroluminescent-CCD Microchip Platform Using Quantum Dot-Peptide Substrates. *Sensors and Actuators B-Chemical.* 2009; 139:13–21.
40. Ganesan R, Mittl PR, Jelakovic S, Grutter MG. Extended Substrate Recognition in Caspase-3 Revealed by High Resolution X-Ray Structure and Analysis. *J Mol Biol.* 2006; 359:1378–1388. [PubMed: 16787777]
41. Delehanty JB, Medintz IL, Pons T, Brunel FM, Dawson PE, Mattoussi H. Self-Assembled Quantum Dot-Peptide Bioconjugates for Selective Intracellular Delivery. *Bioconj Chem.* 2006; 17:920–927.
42. Delehanty JB, Mattoussi H, Medintz IL. Delivering Quantum Dots into Cells: Strategies, Progress and Remaining Issues. *Analytical and Bioanalytical Chemistry.* 2009; 393:1091–1105. [PubMed: 18836855]
43. Venkatesan N, Kim BH. Peptide Conjugates of Oligonucleotides: Synthesis and Applications. *Chem Rev.* 2006; 106:3712–3761. [PubMed: 16967918]
44. Berti L, D'Agostino PS, Boeneman K, Medintz IL. Improved Peptidyl Linkers for Self-Assembling Semiconductor Quantum Dot Bioconjugates. *Nano Research.* 2009; 2:121–129.
45. Prasuhn DE, Deschamps JR, Susumu K, Stewart MA, Boeneman K, Blanco-Canosa JB, Dawson PE, Medintz IL. Polyvalent display and packing of peptides and proteins on semiconductor quantum dots: predicted versus experimental results. *Small.* 2009 In Press.
46. Wang L, Zhang Z, Brock A, Schultz PG. Addition of the Keto Functional Group to the Genetic Code of *Escherichia coli*. *Proc Natl Acad Sci USA.* 2003; 100:56–61. [PubMed: 12518054]
47. Killian JA, Van Cleve MD, Shayo YF, Hecht SM. Ribosome-Mediated Incorporation of Hydrazinophenylalanine into Modified Peptide and Protein Analogues. *J Am Chem Soc.* 1998; 120:3032–3042.
48. Schnolzer M, Alewood P, Jones A, Alewood D, Kent SB. In situ Neutralization in Boc-Chemistry Solid Phase Peptide Synthesis. Rapid, High Yield Assembly of Difficult Sequences. *Int J Pept Protein Res.* 1992; 40:180–93. [PubMed: 1478777]
49. Peng ZA, Peng X. Formation of High-Quality CdTe, CdSe, and CdS Nanocrystals using CdO as Precursor. *J Am Chem Soc.* 2001; 123:183–184. [PubMed: 11273619]
50. Dabbousi BO, Rodriguez-Viejo J, Mikulec FV, Heine JR, Mattoussi H, Ober R, Jensen KF, Bawendi MG. (CdSe)ZnS Core-Shell Quantum Dots: Synthesis and Optical and Structural Characterization of a Size Series of Highly Luminescent Materials. *J Phys Chem B.* 1997; 101:9463–9475.

51. Mei BC, Susumu K, Medintz IL, Delehanty JB, Mountziaris TJ, Mattoussi H. Modular Poly(ethylene glycol) Ligands for Biocompatible Semiconductor and Gold Nanocrystals with Extended pH and Ionic Stability. *J Materials Chemistry*. 2008; 18:4949–4958.
52. Mei BC, Susumu K, Medintz IL, Mattoussi H. Polyethylene Glycol-Based Bidentate Ligands to Enhance Quantum Dot and Gold Nanoparticle Stability in Biological Media. *Nature Protocols*. 2009; 4:412–423. [PubMed: 19265800]

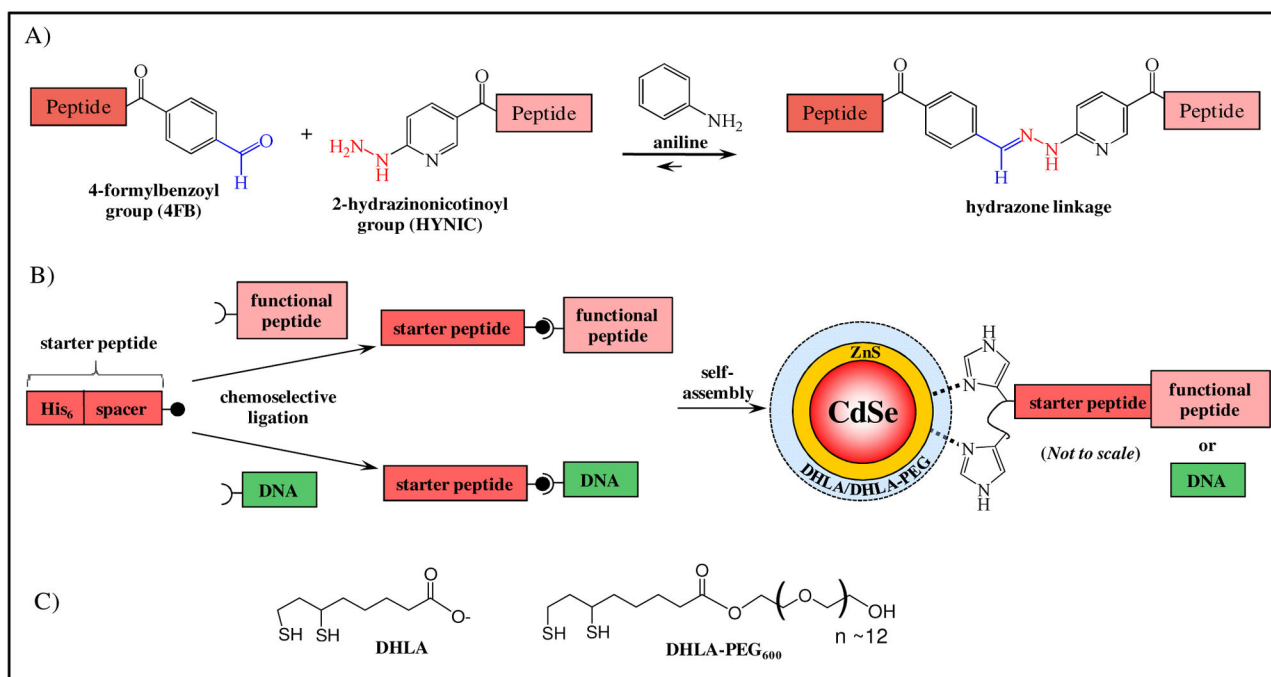


**Figure 1.**

(A) Schematic of the aniline-catalyzed hydrazone ligation between aldehyde and hydrazine functionalities color-coded in blue and red, respectively. (B) Schematic of the two-step, modular design for the attachment of biomolecules to the surface of CdSe/ZnS core/shell QDs surface functionalized with charged DHLA or neutral DHLA-PEG ligands. Initially, a hexahistidine-appended, synthetic, starter peptide is ligated to the appropriately functionalized target biomolecule of interest using chemoselective ligation. Isolated conjugates are then ratiometrically self-assembled to QDs for use in targeted bioassays. (C) Structures of DHLA (deprotonated/negatively charged) and DHLA-PEG<sub>600</sub> QD surface modification ligands.

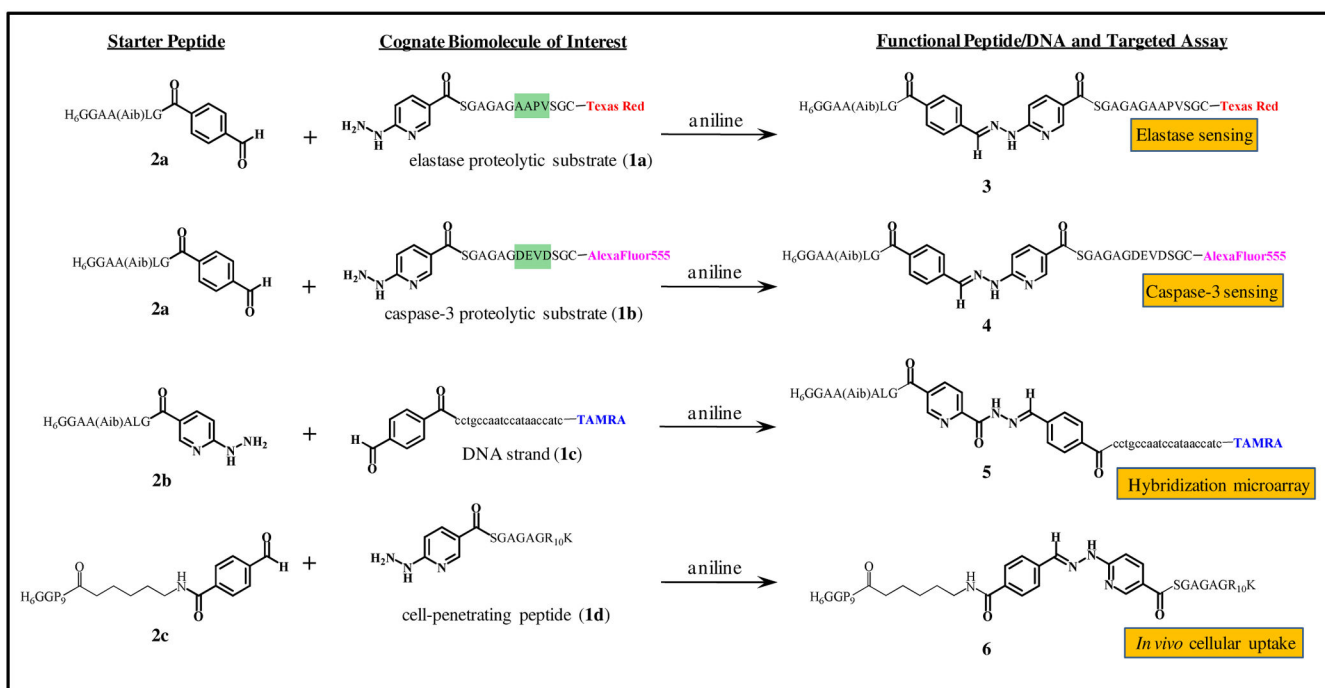


**Figure 2.** Chemical structures of starter and modified peptides (**1a**, **1b**, **1d**), DNA sequence (**1c**), and resulting chemoselective ligates (**3–6**) formed using aniline-catalyzed hydrazone coupling along with the corresponding assays they were assayed in. The location of the proteolytic sites present in **1a,b** are highlighted in green and appropriate dye-labels are shown at the points of linkage to the peptides/DNA.

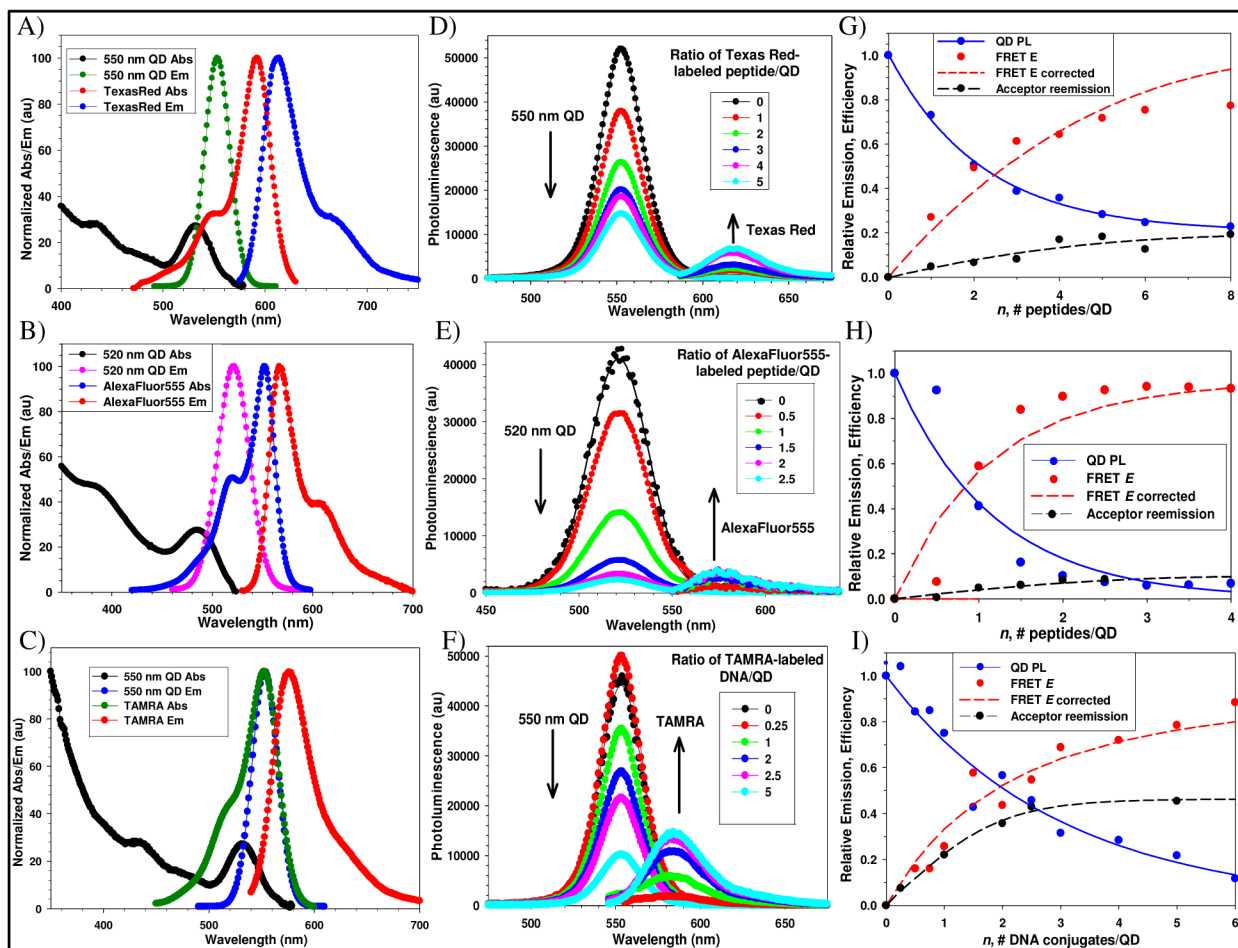


**Figure 3.**

Representative FRET-data for the QD-conjugate systems. Absorption and emission spectra for 550 nm QDs and Texas Red (A), 520 nm QDs and AlexaFluor555 (B), and 550 nm QDs and TAMRA (C). Deconvoluted and direct-acceptor excitation corrected emission spectra for each QD donor-dye-labeled acceptor system for the relevant increasing number of self-assembled peptide conjugate **3** per 550 nm QD (D), peptide conjugate **4** per 520 nm QD (E), conjugate **5** per 550 nm QD (F). QD spectra were fit with a Gaussian profile. Normalized QD PL loss vs.  $n$  (acceptor valence) as indicated, FRET efficiency  $E$ , Poisson-corrected FRET  $E$  and acceptor reemission for each of the QD-conjugate systems are shown in corresponding panels G–I.

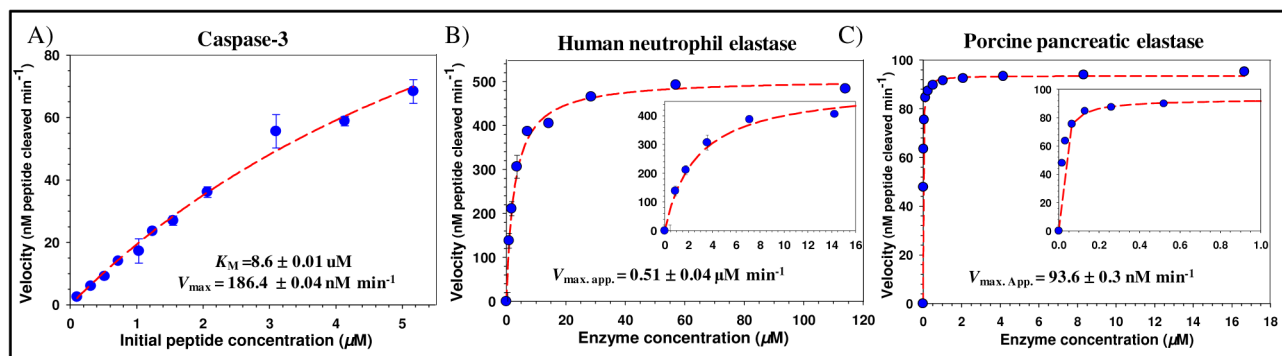


**Figure 4.**

Representative proteolytic activity curves. (A) 520 nm QD DHLA-conjugate **4** assemblies were used to assay recombinant human caspase-3 activity under excess substrate conditions as described. Data from monitoring 580 nm QD DHLA-PEG<sub>600</sub>-conjugate **3** assemblies digested with human neutrophil elastase (B) or porcine pancreatic elastase (C), both in excess enzyme formats. Insets show a close-up of the initial activities at low enzyme concentrations. Estimated  $K_M$  and  $V_{max}$  values derived for caspase-3 are shown along with the  $V_{max, app.}$  for the elastase assays.

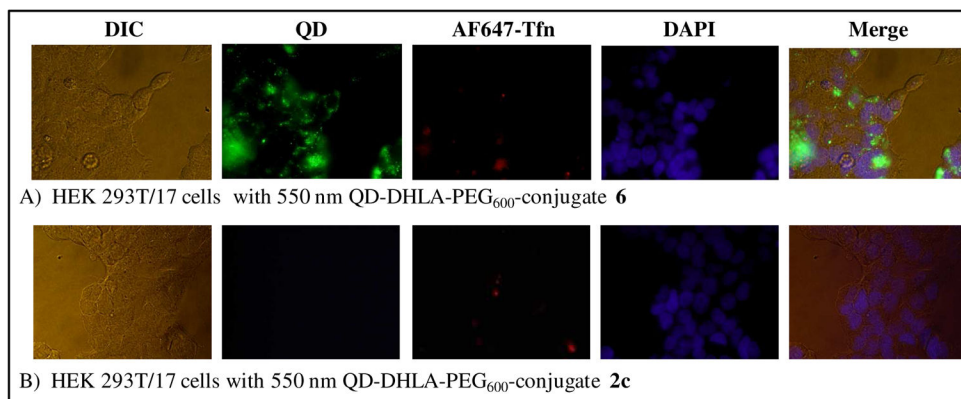


**Figure 5.**

Representative images of HEK 293T/17 cells incubated at 37°C for 1 hour with 50 nM of 550 nm QD DHLA-PEG<sub>600</sub> conjugated to CPP-ligate **6** (A) or starter peptide **2c** (B) as a control. For each panel the corresponding differential interference contrast (DIC), QD fluorescence (~550 nm), AF647-Tfn fluorescence (~670 nm), DAPI fluorescence (~460 nm), and merged composite images are shown.

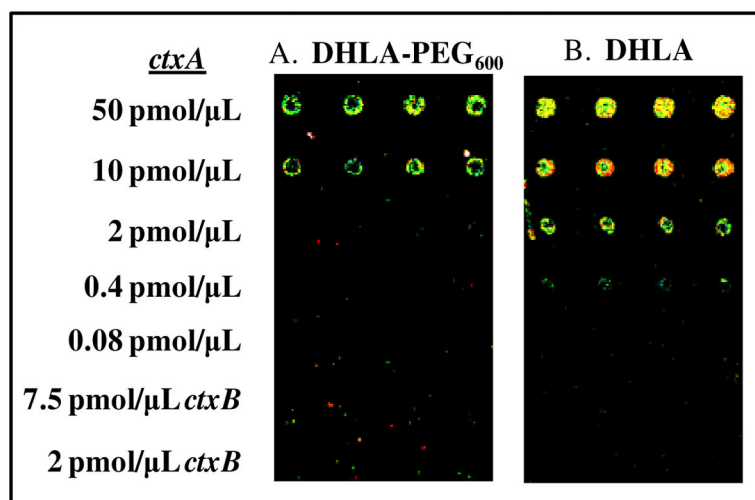


**Figure 6.** Images of microarrays hybridized with peptido-DNA ligate **5** self-assembled to 550 nm QDs surface functionalized with DHLA-PEG<sub>600</sub> (A) or DHLA (B). The slides were pre-spotted with varying concentrations of the *ctxA* sequence (0.08–250 pmol/μL, four replicate spots). Note, *ctxB* spots were used as a negative control.

Selected photophysical and FRET properties of each QD-donor dye-acceptor conjugate pair examined. Quantum yields (QY) of the QDs were ~20% and QD radii were estimated from ref<sup>49</sup>.

**Table 1**

QD donor $\lambda_{em}$ (nm)	Surface Ligand	QD core/shell radius (Å)	Acceptor dye-labeled ligates	Dye $\lambda_{abs}/\lambda_{em}$ (nm)	Dye Ext. Coeff. ( $M^{-1} cm^{-1}$ )	$R_0$ (Å)	$r$ (Å)
520	DHLA	27–28	Caspase-3 substrate-AlexaFluor555 (4)	555/565	150,000	45	33
550	DHLA	30–31	Peptide/DNA-TAMRA (5)	555/580	65,000	51	53
550	DHLA	30–31	Elastase substrate-Texas Red (3)	595/615	80,000	46	30
580	DHLA-PEG <sub>600</sub>	33–34	Elastase substrate-Texas Red (3)	595/615	80,000	48	66